*J. Fluid Mech.* (1982), *vol.* 125, *pp.* 75–97
*Printed in Great Britain*



# Single-mode theory of diffusive layers in thermohaline convection

By D. O. GOUGH

Institute of Astronomy and Department of Applied Mathematics and Theoretical Physics, University of Cambridge, Silver Street, Cambridge CB3 9EW

AND JURI TOOMRE

Joint Institute for Laboratory Astrophysics, and Department of Astrophysical, Planetary and Atmospheric Sciences, University of Colorado, Boulder, CO 80309

(Received 20 December 1979 and in revised form 11 June 1982)

A two-layer configuration of thermohaline convection is studied, with the principal aim of explaining the observed independence of the buoyancy-flux ratio on the stability parameter when the latter is large. Temperature is destabilizing and salinity is stabilizing, so diffusive interfaces separate the convecting layers. The convection is treated in the single-mode approximation, with a prescribed horizontal planform and wavenumber. Surveys of numerical solutions are presented for a selection of Rayleigh numbers $R$, stability parameters $\lambda$ and horizontal wavenumbers $a$. The solutions yield a buoyancy flux ratio $\chi$ that is insensitive to $\lambda$, in accord with laboratory experiments. However $\chi$ increases with increasing $R$, in contradiction to laboratory observations.

## 1. Introduction

Thermohaline convection is distinguished from Bénard convection by its occurrence even when the overall density increases with depth, provided temperature and salinity make opposing contributions to the density. There is a striking tendency for the motion to build stepped profiles in both heat and salt. Such structures have been observed in the laboratory, and there is strong evidence that they exist in lakes and oceans. They may be important also in the cores of evolved stars.

The overall structure of the flow depends upon whether temperature or salinity destabilizes (the other stabilizes). With temperature destabilizing, the flow in laboratory experiments develops into a series of horizontal layers of convection, each separated from its neighbour by a relatively sharp interface within which temperature and salinity vary rapidly. This situation is frequently called 'diffusive layering', since the overall transport of heat and salt is controlled by diffusion through the interfaces.

The linear and finite-amplitude stability theory needed to explain the onset of some forms of thermohaline convection now appears to be understood (Stern 1960; Baines & Gill 1969; Veronis 1965, 1968; Huppert & Moore 1976), and it is clear that instability can arise because of the differing molecular diffusivities of heat and salt. However, this theory is of little help once vigorous motions have been established, and our impressions then are derived mainly from simple laboratory experiments.

This paper is concerned with trying to provide a nonlinear theory to interpret the experiments on diffusive layering. The configuration that we model is much like that of the experiments by Turner (1965, 1968), with convection occurring in two horizontal layers separated by a diffusive interface. The lower layer is warmer, saltier and denser than the upper layer.

## 2. Experiments and explanations

Most of the two-layer experiments have been modelled on the initial studies by Turner (1965). These include the work of Broughton (1972), Crapper (1973, 1975), Marmorino (1974) and Marmorino & Caldwell (1976). A good review of thermohaline convection experiments is provided by Turner (1973, chap. 8). Initially two uniform layers of water fill the apparatus, the lower being the more saline. Heat is supplied through the bottom boundary which drives convection in both layers. Provided the heating rate is not too great, the convective motions do not traverse the boundary separating the layers, and a diffusive interface is maintained. The centres of the two layers of convection are separated in depth by $d$; over this distance the temperature changes by $\Delta T$ and salinity by $\Delta S$, though they do so mainly across the interface. Since the boundaries are impervious to salt, $\Delta S$ decreases slowly with time. The interface is characterized by a stability parameter

$$\lambda = \frac{\alpha_s \Delta S}{\alpha \Delta T}, \tag{2.1}$$

where $\alpha$ and $\alpha_s$ are defined such that $-\alpha\Delta T$ and $\alpha_s \Delta S$ are the density increments resulting from changes of $\Delta T$ and $\Delta S$ in temperature and salinity; $\lambda > 1$ since the lower layer is always denser than the upper layer.

Turner made measurements to see how the stability parameter $\lambda$ influénces the vertical fluxes $F$ and $F_s$ of heat and salt through the interface. His most-striking result concerns the buoyancy-flux ratio

$$\chi = \frac{\alpha_s F_s}{\alpha F}, \tag{2.2}$$

which is also the ratio of the potential-energy changes due to the transfer of salt and heat across the interface. Turner found that $\chi$ was nearly constant when $\lambda \gtrsim 2$, irrespective of heating rate, at a value $\chi_c$ of about 0·15. As $\lambda$ was decreased below 2, $\chi$ increased, and approached unity as $\lambda \to 1$. Since these were run-down experiments, a range in $\lambda$ could be sampled as $\Delta S$ and $\lambda$ decreased in time.

Crapper (1973, 1975) repeated Turner's experiments and, though he found some changes in the behaviour of $\chi$ at the small-$\lambda$ turnoff, the insensitivity of $\chi$ to $\lambda$ at larger values persisted. Marmorino (1974) and Marmorino & Caldwell (1976) carried out similar experiments over a wider range of heat fluxes, achieving this by cooling their apparatus from above in addition to heating from below. They too found that $\chi$ was relatively insensitive to $\lambda$, although $\chi_c$ did depend on heat flux. For their lowest heat flux ($F \approx 10^{-4}$ cal cm$^{-2}$ s$^{-1}$) $\chi_c$ was near 0·40, and it decreased steadily to 0·15 as the heat flux approached that of Turner's experiments ($F \approx 5 \times 10^{-2}$).

Just what happens near $\lambda = 2$ is uncertain. All the experimenters report that the interfaces tend to sustain waves, and some report that they migrate vertically. It appears that the interface begins to break down when $\lambda \lesssim 2$, but little quantitative experimental information is available.

Another important issue is the variation of the heat flux $F$ as the stability parameter $\lambda$ changes. The double-layer experiments by Turner (1965) show that $F$ decreases with increasing $\lambda$, the heat transport at $\lambda = 7$ being only about 10% of that at $\lambda = 2$. Marmorino & Caldwell (1976) report that $F$ seems to be independent of $\lambda$ at large $\lambda$ ($\lambda \gtrsim 10$). Despite some differences in the measured values of $F$, the experimenters agree that increasing the stabilizing salinity gradient decreases the heat flux substantially. This behaviour was found also in the experiments by Griffiths (1979*a*, *b*) on diffusive interfaces formed in the presence of several dissolved salts.

Diffusive layering seen in the laboratory has not been explained adequately by theory. Progress may be made with kinematical studies, assuming a particular form for the turbulent velocity field and trying to compute its effects on the density interface, in the manner of Linden (1973). But we prefer instead to investigate dynamical models of convection, even if they are rather crude, in which the velocity, temperature and salinity are directly linked. We formulate such an approach in §3. After posing the problem, we begin by outlining a theoretical procedure that has been used in dealing with thermal convection, and then we display the equations that result from extending this method to the thermohaline case.

## 3. Treatment of the problem

We consider thermohaline convection occurring in two adjacent horizontal layers separated by a diffusive interface. This configuration resembles the double-layer laboratory experiments originally performed by Turner (1965). In particular, we study motions that result in a region of fluid of overall depth $2d$ bounded by two horizontal planes on which suitable velocity, temperature and salinity boundary conditions are imposed. A fluid in Boussinesq approximation is considered, with the density $\rho$ satisfying $\rho = \rho_0[1-\alpha(T-T_0)+\alpha_s(S-S_0)]$. The lower boundary is maintained at constant temperature $T = T_0+\Delta T$ and constant salinity $S = S_0+\Delta S$, and the upper boundary at $T = T_0-\Delta T$ and $S = S_0-\Delta S$. Here $\Delta T$, $\Delta S > 0$, and are chosen such that $\alpha_s \Delta S > \alpha \Delta T$.

The problem can be described in terms of the thermal Rayleigh numbers

$$R = \frac{g\alpha \Delta T d^3}{\kappa \nu}, \quad R_s = \frac{g\alpha_s \Delta S d^3}{\kappa_s \nu}. \tag{3.1}$$

Note that $\kappa_s$ is used in the definition of $R_s$. We shall also require

$$\sigma = \frac{\nu}{\kappa}, \quad \tau = \frac{\kappa_s}{\kappa}. \tag{3.2}$$

The stability parameter or density-anomaly ratio (2.1) can then be expressed as

$$\lambda = \frac{\tau R_s}{R}. \tag{3.3}$$

Here $g$ is the gravitational acceleration, $\nu$ is the kinematic viscosity, and $\kappa$ and $\kappa_s$ are the diffusivities of heat and salt. All these are assumed to be constant. We shall hereafter use a dimensionless formulation using $d$, $d^2/\kappa$, $\Delta T$ and $\Delta S$ as units of length, time, temperature and salinity. The diffusivity ratio $\tau$ for this system is taken to be $10^{-2}$ and the Prandtl number $\sigma$ is 6·8.

### 3.1. *Modal equations*

We represent the flow by the modal approximation. The equations result from expanding the fluctuating velocity and temperature fields in a truncated set of planform functions of the horizontal coordinates. The severest truncation retains only one term and yields the single-mode equations. These contain a parameter $C$ that characterizes the shape of the planform and a wavenumber $a$ that defines its scale. Both must be specified arbitrarily. Toomre, Gough & Spiegel (1977, hereinafter II) have obtained numerical solutions of the single-mode equations at moderate values of the Rayleigh number $R$; asymptotic solutions at high $R$ are presented by Gough, Spiegel & Toomre (1975*a*, hereinafter I). It was found in II that, with a suitable choice

of the wavenumber $a$, the solutions can be made to replicate the heat transport and yield mean-temperature profiles and amplitudes of motion not unlike those in the laboratory experiments. This gives us some encouragement to proceed to a study of thermohaline convection under the same approximation.

As in I we first decompose the fluid temperature $T$ and salinity $S$ into mean and fluctuating parts: $T = \bar{T} + \theta$ and $S = \bar{S} + \phi$, where the overbar denotes a horizontal average. The velocity $\mathbf{u}$ is written in the form

$$\mathbf{u} = \left(a^{-2}\frac{\partial W}{\partial z}\frac{\partial f}{\partial x}, a^{-2}\frac{\partial W}{\partial z}\frac{\partial f}{\partial y}, Wf\right), \tag{3.4}$$

which satisfies the continuity equation and precludes a vertical component of vorticity. The temperature and salinity fluctuations take the forms

$$\theta = \Theta f, \quad \phi = \Phi f. \tag{3.5}$$

The amplitude functions $W$, $\Theta$ and $\Phi$ depend on $z$ and $t$ alone, and the horizontal planform $f(x, y)$ satisfies

$$\frac{\partial^2 f}{\partial x^2} + \frac{\partial^2 f}{\partial y^2} = -a^2 f, \quad \overline{f^2} = 1. \tag{3.6}$$

Here $(x, y, z)$ are spatial Cartesian coordinates with $z$ vertical, and $t$ is time. These forms for $\mathbf{u}$, $\theta$ and $\phi$ are substituted into the equations of motion, which are subsequently horizontally averaged, or multiplied by $f$ and then averaged, just as in I. The resulting equations, after elimination of pressure and horizontal velocity components, are the horizontal vorticity equation

$$\left(\frac{1}{\sigma}\frac{\partial}{\partial t} - \mathscr{D}\right)\mathscr{D}W + Ra^2(\Theta - \lambda\Phi) = -\frac{C}{\sigma}\left(2\frac{\partial W}{\partial z}\mathscr{D}W + W\mathscr{D}\frac{\partial W}{\partial z}\right), \tag{3.7}$$

the fluctuating-thermal-energy equation

$$\left(\frac{\partial}{\partial t} - \mathscr{D}\right)\Theta + \frac{\partial \bar{T}}{\partial z}W = -C\left(2W\frac{\partial \Theta}{\partial z} + \Theta\frac{\partial W}{\partial z}\right), \tag{3.8}$$

the fluctuating-salinity equation

$$\left(\frac{\partial}{\partial t} - \tau\mathscr{D}\right)\Phi + \frac{\partial \bar{S}}{\partial z}W = -C\left(2W\frac{\partial \Phi}{\partial z} + \Phi\frac{\partial W}{\partial z}\right), \tag{3.9}$$

the mean-thermal-energy equation

$$\left(\frac{\partial}{\partial t} - \frac{\partial^2}{\partial z^2}\right)\bar{T} = -\frac{\partial}{\partial z}(W\Theta), \tag{3.10}$$

and the mean-salinity equation

$$\left(\frac{\partial}{\partial t} - \tau\frac{\partial^2}{\partial z^2}\right)\bar{S} = -\frac{\partial}{\partial z}(W\Phi), \tag{3.11}$$

where

$$\mathscr{D} \equiv \left(\frac{\partial^2}{\partial z^2} - a^2\right), \quad C = \tfrac{1}{2}\overline{f^3}.$$

Setting the self-interaction parameter $C$ to zero yields what are commonly called the single-mode mean-field equations. Within a single-mode representation, rolls and rectangular planforms have no self-interaction ($C = 0$), but a hexagonal planform has $C = \sqrt{\frac{1}{6}} = 0{\cdot}408$.

When the solutions are steady, $\partial/\partial t = 0$ and the mean equations (3.10) and (3.11) have the first integrals

$$\beta + W\Theta = N, \tag{3.12}$$

$$\gamma + W\Phi = M \equiv \mu N, \tag{3.13}$$

where

$$\beta = -\frac{\partial \overline{T}}{\partial z}, \quad \gamma = -\frac{\partial \overline{S}}{\partial z}.$$

The constants of integration are the Nusselt number $N$ and the salinity flux $M$, the latter being measured in units of $\kappa_s \Delta S/d$; their ratio is $\mu = M/N$. The buoyancy-flux ratio may thus be expressed as

$$\chi = \tau\lambda\mu.$$

Note that only when $C \neq 0$ do the steady equations contain the Prandtl number $\sigma$.

### 3.2. *Boundary conditions*

We assume that the boundaries are perfect thermal conductors and salinity reservoirs, with prescribed constant boundary temperatures and salinities:

$$\left.\begin{aligned} T = \overline{T} = 1, \quad S = \overline{S} = 1 \quad (z = 0), \\ T = \overline{T} = -1, \quad S = \overline{S} = -1 \quad (z = 2), \end{aligned}\right\} \tag{3.14}$$

which requires that

$$\theta = \Theta = 0, \quad \phi = \Phi = 0 \quad (z = 0, 2). \tag{3.15}$$

We have chosen the upper boundary to be at $z = 2$ because we are studying two layers. Usually we adopt the so-called 'free' boundary conditions of convection theory, which presume that the horizontal viscous stresses and the $z$-component of velocity vanish, thus yielding the conditions

$$W = \frac{\partial^2 W}{\partial z^2} = 0 \quad (z = 0, 2). \tag{3.16}$$

We have also computed solutions subject to the rigid condition $\mathbf{u} = \mathbf{0}$ on the boundaries, which requires that (3.16) be replaced by

$$W = \frac{\partial W}{\partial z} = 0 \quad (z = 0, 2). \tag{3.17}$$

Of course we could have chosen boundary conditions that mimic the experiments more directly. The choice (3.14)–(3.16) was made because with them the system can be regarded as part of a larger multilayer system. Indeed, even the steady two-layer state can be studied by considering just one of the convective layers (say the lower one). This is so because it is a property of the numerical solutions presented in §4 that, at the centre of a steady diffusive interface, $W$, $\partial^2 W/\partial z^2$, $\Theta$ and $\Phi$ all vanish. These are precisely our boundary conditions (3.15) and (3.16). A time-independent uniformly layered medium with diffusive interfaces, in modal approximation, is therefore equivalent to a stack of convective layers, each of which is confined by free boundaries. When $C \neq 0$ alternate layers are reflections of each other about the midplane of the diffusive layer that separates them. Therefore, in particular, they each have the same depth. When $C = 0$ the solutions in every layer are identical because each is symmetrical about its own midplane. Thus the values of $R$ and $\lambda$ characterizing a single layer within a stack are just the ones defined here. We shall study this particular case by replacing the boundary conditions (3.15) and (3.16) at $z = 2$ by identical ones imposed at $z = 1$, and by requiring that $\overline{T} = 0$ and $\overline{S} = 0$ at $z = 1$ in place of the upper boundary condition in (3.14).

### 3.3. *Numerical procedure*

The governing equations have been solved numerically by finite differences using the methods discussed in appendix A of II, typically with 300 grid points. Two independent programmes were used, one solving the time-dependent equations and the other solving the steady equations with $M$ and $N$ as eigenvalues. Both methods incorporated the first-derivative mesh-stretching scheme of Gough, Spiegel & Toomre (1975*b*).

## 4. Properties of the numerical solutions

Time-dependent numerical experiments were performed from a variety of initial conditions. In some we started with an isothermal state, at the temperature of the upper boundary, and a uniform stable salinity gradient. By perturbing this with low-amplitude fluctuations we were able to model the formation and growth of convective layers near the lower plate, similar to those first observed in the experiments of Turner & Stommel (1964). In other computations the initial mean fields were step-like, so as to model laboratory experiments started from a stepped structure that had been achieved by mechanical mixing. It was the latter class of experiments that interested us the most, since in these the diffusive interfaces were quasi-stationary and measurements of fluxes were possible. We have adopted boundary conditions that permit truly steady solutions, and when we obtained them from a time-dependent integration, we started most often from existing steady solutions with different $R$, $\lambda$ or $a$. Sometimes noise was added to test whether the final state to which the system evolves depends on initial conditions. All our solutions were obtained for values of $R \geqslant 1{\cdot}25 \times 10^5$.

Most of our study concerns the steady solutions, and these we discuss in some detail below. For the double-layer systems that we have computed explicitly, such as those illustrated in figure 1, it is convenient to introduce an effective stability parameter $\lambda_e$ that characterizes the central interface, defined by

$$\lambda_e = \frac{\alpha_s[\bar{S}(\tfrac{1}{2}) - \bar{S}(\tfrac{3}{2})]}{\alpha[\bar{T}(\tfrac{1}{2}) - \bar{T}(\tfrac{3}{2})]}\lambda.$$

The flux ratio in the steady interface is, of course, the same as that for the entire system.

We have distinguished two quite different types of interface, which we have called A and B. Interfaces of type A exist only when $\lambda_e$ is small, and are characterized by a buoyancy-flux ratio $\chi \approx \tau^{\frac{1}{2}}\lambda_e$, irrespective of $R$, $a$, $\sigma$ and $C$. Their structure is quite simple and the $\tau$-dependence reflects simply the ratio of the rates of diffusion of salinity and temperature. Interfaces of type B are more complicated, and exist at larger values of $\lambda_e$. The associated values of $\chi$ are lower than the type A formula would predict, and are relatively insensitive to $\lambda_e$. They too exist over a wide range of wavenumbers, for both rolls and hexagons, but $\chi$ now does depend on $R$, $a$ and $C$ (see figures 3 and 4).

The rest of this section is devoted to a more detailed discussion of the properties of the solutions, all of which have $\sigma = 6{\cdot}8$ and $\tau = 10^{-2}$. Our most-extensive surveys have $C = 0$.

### 4.1. *Description of double-layer hexagons*

Three steady solutions are illustrated in figure 1. The convection is three-dimensional, with the interaction parameter $C = 0{\cdot}408$ characteristic of hexagonal planforms; the

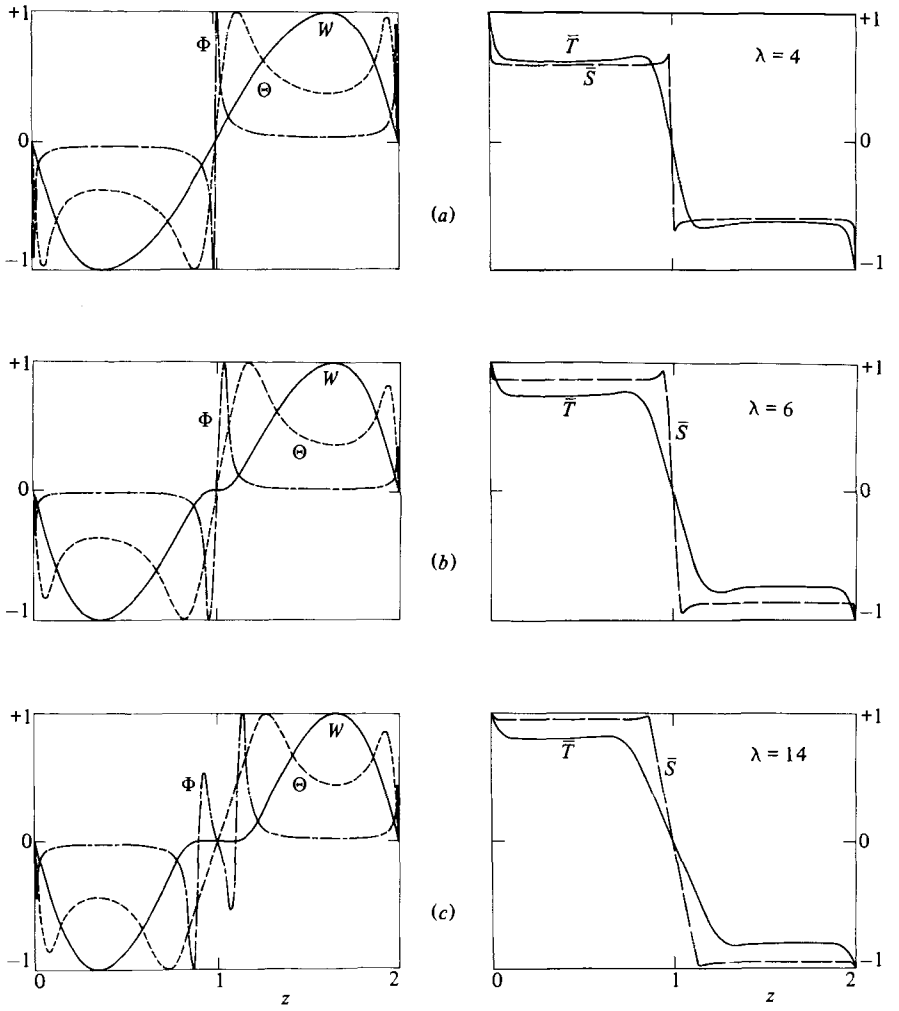


FIGURE 1. Amplitudes of vertical velocity $W$ and fluctuations $\Theta$ and $\Phi$ of temperature and salinity, measured in units of their maximum values $W_0$, $\Theta_0$ and $\Phi_0$, and the corresponding mean temperature $\bar{T}$ and mean salinity $\bar{S}$, plotted against the vertical coordinate $z$ on uniform scale for three values of the stability parameter $\lambda$. The solutions are for hexagons subject to free boundary conditions; $R = 1{\cdot}25 \times 10^5$, $\sigma = 6{\cdot}8$, $\tau = 10^{-2}$ and $a = 4$. The stability parameters, Nusselt numbers, buoyancy-flux ratios and scaling factors are as follows: (*a*) $\lambda = 4$, $N = 7{\cdot}97$, $\chi = 0{\cdot}412$, $W_0 = 190{\cdot}6$, $\Theta_0 = 0{\cdot}110$, $\Phi_0 = 0{\cdot}118$; (*b*) 6, 5·07, 0·292, 154·2, 0·090, 0·105; (*c*) 14, 3·31, 0·307, 111·2, 0·068, 0·028.

sign of $W$ in the solutions shown in figure 1 is such as to correspond to plumes rising in the lower layer and falling in the upper towards the diffusive interface at $z = 1$. The solution in figure 1(*a*) has a type A interface; those in figures 1(*b*, *c*) have interfaces of type B.

The structure of the fields in figure 1(*a*) is reminiscent of those encountered in ordinary thermal convection (see the single-mode solutions in figure 1 of II), although of course here there is an overall decrease of density with height due to the stabilizing influence of salt. Within each convective layer the vertical velocity amplitude $W$ is smooth and has a single maximum. Away from the boundary layers most of the heat is transported by convection; $\bar{T}$ is nearly constant and $W\Theta \approx N$ (cf. (3.14)). Therefore the temperature fluctuation $\Theta$ varies inversely with $W$, and significant deviations

from this behaviour occur only in the boundary layers where thermal conduction is important and where $\Theta$ turns over and then drops to zero. The mean temperature gradient $\beta$ becomes comparable to the convective heat flux $W\Theta$ where $\Theta$ peaks, and it reaches its maximum magnitude $N$ at $z = 0$, 1 and 2 where both $W$ and $\Theta$ vanish.

The salinity fields $\bar{S}$ and $\Phi$ in figure 1 ($a$) are similar to $\bar{T}$ and $\Theta$, though the boundary layers in salinity are narrower by a factor of 10; this is a property of all type A interfaces. The boundary-layer thicknesses are simply proportional to the square roots of the appropriate diffusivities. The salt flux $M$ is dominated by the convective term $W\Phi$ in the interior, and by the mean salinity gradient $\gamma$ in the boundary layers.

The interfaces centred at $z = 1$ in figures 1 ($b$, $c$) are typical examples of type B. They are rather broader than their type A counterpart. It is evident from the positions of the peaks in $\Theta$ and $\Phi$ that the ratio of the thermal and haline boundary-layer thickness is no longer as great as 10; in the example illustrated with $\lambda = 6$ this ratio is 3·7, and in the solution with $\lambda = 14$ it is only 1·7. The vertical velocity amplitude $W$ is small throughout the interface, and close inspection of the solution at $\lambda = 14$ reveals two weak countercells within the central region of the interface. The $\Theta$-field still varies almost linearly in this region, but $\Phi$ has developed an additional pair of peaks. It should be remarked that, very near to $z = 1$, $W$ is proportional to $z$, as is clearly the case in interfaces of type A (see figure 1 $a$). Thus the horizontal stress vanishes at $z = 1$ in all steady solutions.

Type B interfaces are found only when the stability parameter $\lambda$ is sufficiently large (see figure 2). Significant stabilization of the flow can then occur within the haline boundary layer, thereby reducing the magnitude of the vertical velocity to quite small values. In the thermal boundary layers, $W$ at first increases approximately quadratically with distance; such a variation is rather like that of thermal convection with rigid boundary conditions (3.19) on the velocity. Although the midplane of the diffusive interface is actually stress-free, the effects of the strong negative buoyancy in the thin haline boundary layer are such as to make the velocity appear to be experiencing rigid conditions.

In figures 1 ($b$, $c$) it is evident that only the central interface is of type B. Thus if these solutions are considered to be part of a multilayer configuration, the interfaces would alternate between type A and type B. Another possibility might be that all the interfaces are of type B, but we have found such solutions only when $C = 0$. The solutions with $C = 0$ are superficially similar to those with hexagonal planforms, the principal difference being that each convecting layer is symmetrical about its midplane.

Finally we remark that all the double-layer steady solutions subject to free boundary conditions that we obtained as final states of a time evolution had reflectional symmetry about $z = 1$, whatever the initial conditions. We used this result when we subsequently computed steady solutions directly, by computing only a single convection layer with stress-free boundary conditions at $z = 0$ and $z = 1$. Because of the further symmetry possessed by solutions with $C = 0$, one need compute only half a layer in this case.

### 4.2. *Domains of existence of steady solutions*

The domains within which solutions of types A and B are found are shown in figure 2. Solutions of one type or other can be found at all values of $\lambda$ and $a$ within the confines of the figure. The boundaries vary with $R$ and $C$, though the main qualitative features of the diagram appear to be preserved. Type A solutions exist from $\lambda = 0$

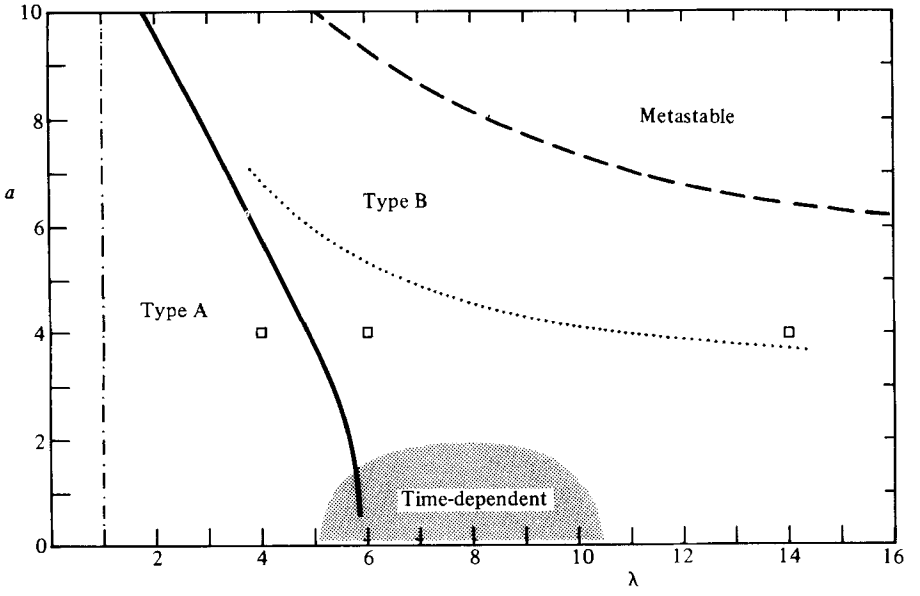


FIGURE 2. Domains of existence in $(a, \lambda)$ of hexagon-solution types subject to free boundary conditions when $R = 1{\cdot}25 \times 10^5$, $\sigma = 6{\cdot}8$ and $\tau = 10^{-2}$. Steady solutions of type A exist only to the left of the continuous line, solutions of type B to the right. To the left of the dot–dashed line, where $\lambda < 1$, the density stratification is unstable; a steady double-layer solution, if perturbed, reverts to a single convection cell extending over the entire layer. In the shaded domain the solutions are unstable to migration and eventual dissolution of the central interface. Above the dashed line the solutions are metastable. The dotted line locates the wavenumber $a_m$ at which the buoyancy flux $(1-\chi)N$ is maximized at constant $R$ and $\lambda$. The positions of the three solutions illustrated in figure 1 are marked with squares. About 200 numerical solutions were used to determine the domains shown here, with the densest sampling near the transition lines. The corresponding diagram for rolls is similar.

to a value of $\lambda$ that decreases as $a$ increases, though when $\lambda < 1$ they are certainly unstable. Solutions with interfaces of type B exist at higher values of $\lambda$. The domains appear not to overlap when free boundary conditions are applied, though there is some overlap for solutions subject to rigid boundary conditions.

Note that the abscissa in figure 2 is $\lambda$ and not $\lambda_e$. Provided that $\lambda$ is well above the value at which the transition between the two types of solution occurs, $\lambda_e$ for the type B interface is close to $\lambda$, whereas for the corresponding type A interface it is of course considerably smaller. This is the case not only for the hexagons represented in figure 2, but also for rolls (cf. figure 4). An immediate consequence of this property is that when both types of interface coexist (as in the $\lambda = 6$ and 14 solutions of figure 1), the condition that they must each transport the same fluxes implies that the type B interface always accommodates most of the variation in $\overline{S}$ and $\overline{T}$. However, when the interfaces are both of type A, both values of $\lambda_e$ are identical and equal to $\lambda$. Interfaces of type B arise at the midplanes ($z = 1$) of our two-layer systems rather than at the boundaries merely as a result of our initial conditions. For brevity, in the discussion that follows we shall designate our entire solutions as being simply of type A or B according to the character of the central interface.

In addition to the steady solutions described above, two other categories of solutions exist. The shaded area in figure 2 is the domain of time-dependent solutions in which the central interface migrates either upwards or downwards. During the

evolution one of the convection layers expands at the expense of the other, the final state being one in which a single layer of convection fills the entire region of fluid. Although steady solutions do exist in the shaded domain in figure 2, our limited stability studies showed that they are unstable to finite-amplitude disturbances. Initially the migration velocity increases exponentially, with an $e$-folding time that is comparable to the thermal diffusion time $d^2/\kappa$ and which increases with $\lambda$. By the time the interface has moved some 30–40 % of the depth of a single convective layer its velocity is comparable to the characteristic haline diffusion velocity $\kappa_s/d$. Its velocity then increases much more rapidly, and the interface disintegrates as the larger convective layer consumes the smaller.

The other category of solutions lies to the upper right of the dashed line in figure 2. As both $a$ and $\lambda$ are increased, the type B interface assumes an increasingly complicated structure, much like the $\lambda = 14$ solution shown in figure 1 ($c$). Above the dashed transition line we find that such solutions are metastable: perturbing the steady solutions can lead to a broadening of the middle region accompanied by a growth in the amplitudes of the two embedded countercells; alternatively, the solution there may evolve to a state with several weak countercells. Close to the transition line the time evolution terminates in one of several steady solutions, which differ mainly in the structures of their interfaces. At higher $a$ and $\lambda$ the central region can continue to expand slowly until it fills the entire space, thereby suppressing the convection entirely in the adjacent layers. Eventually a new multilayer structure with less vigorous convection replaces the former; we have not studied these states in much detail. Outside the time-dependent and metastable regions the steady solutions are stable to small-amplitude perturbations provided that $\lambda > 1$.

### 4.3. *Buoyancy-flux ratios*

The dependence of $\chi$ on $\lambda$ is shown in figures 3 and 4. The linear branches through the origin correspond to type A solutions; they extend uniformly from the unstably stratified domain of ordinary thermal convection ($\lambda = 0$) to the gravitationally stable domain of double-diffusive flow. The nearly horizontal branches at high $\lambda$ correspond to solutions of type B.

At first sight the transition in figure 3 from type A to type B suggests a bifurcation of solutions, judging from the behaviour of the $a = 3$ solutions in the vicinity of $\lambda = 5{\cdot}35$. We have not been able to establish whether this is actually the case, but we suspect not because we have failed to find an extension of an A-branch beyond the transition. We have resolved the transition sufficiently to demonstrate that it is smooth, and is not a cusp catastrophe as one might expect from its appearance in figure 3. The smoothness of the transition is more evident in figure 4. This is a result of increasing $R$, rather than decreasing $C$.

Type B solutions yield a buoyancy flux ratio whose slow variation with $\lambda$ bears some resemblance to the laboratory data. However, the value of $\chi$ does depend on the wavenumber, and it is not clear which $a$ to choose. Although all limited modal representations are subject to this difficulty, we found in our single-mode analysis of thermal convection in II that the solutions that do best in comparisons with laboratory results are close to those that maximize the heat transport. A close analogue in the thermohaline problem is the buoyancy flux, which is proportional to $(1-\chi)N$. Thus we have varied the wavenumber $a$ (at fixed $R$ and $\lambda$) in order to locate the value, say $a_m$, at which $(1-\chi)N$ is maximized. This is our 'preferred' solution, though the choice is somewhat arbitrary. In the type B solution the value of $a_m$ usually lies close to that which maximizes the heat flux $N$. The resulting flux

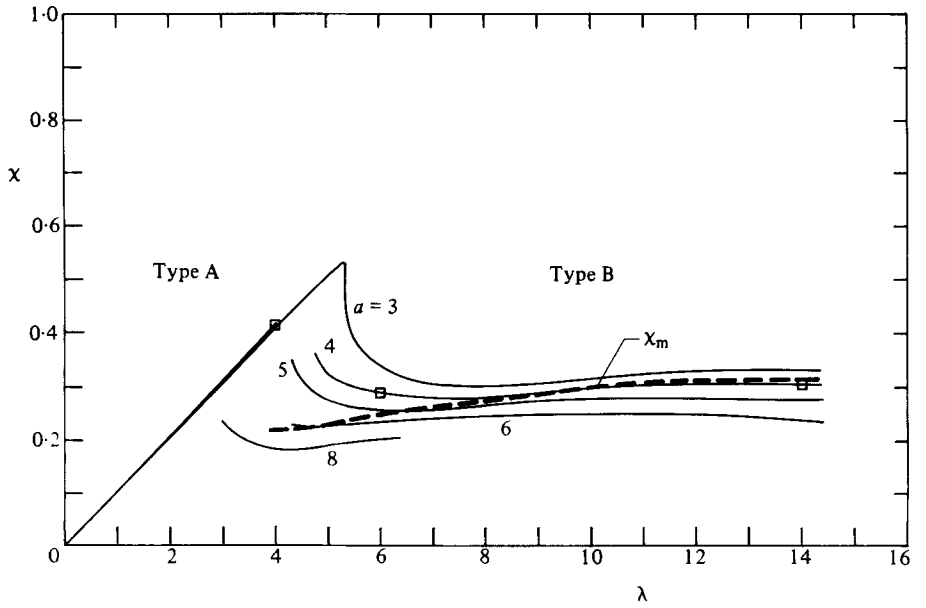


FIGURE 3. Buoyancy-flux ratios $\chi$ for double-layer hexagons subject to free boundary conditions; $R = 1{\cdot}25 \times 10^5$, $\sigma = 6{\cdot}8$ and $\tau = 10^{-2}$. The continuous lines represent solutions at the fixed wavenumbers indicated. The dashed line denotes $\chi_m$: its value increases slowly with $\lambda$, from 0·22 at $\lambda = 4$ (where $a_m = 6{\cdot}8$) to 0·32 at $\lambda = 14$ ($a_m = 3{\cdot}7$). The associated Nusselt number $N_m$ decreases with $\lambda$ in this interval from 5·1 to 3·4; the maximum Nusselt number, at $\lambda = 0$, is 10·7. The surveys are too sparse to determine $\chi_m$ when $\lambda < 4$. The almost-straight line passing through the origin results from solutions of type A; here $\lambda$ is also equal to the effective stability parameter $\lambda_e$ characterizing each diffusive layer. The horizontal branches correspond to solutions with a central interface of type B; for these $\lambda_e$ for the central interface is close to $\lambda$, and that for the other boundary layers is where the type A branch yields the same value of $\chi$. The squares locate the solutions illustrated in figure 1.

ratio $\chi_m \equiv \chi(a_m)$ is indicated by the dashed curves in figures 3 and 4. It is greater than the constant experimental value of 0·15 reported by Turner (1965) and Crapper (1973, 1975), though close to that reported by Marmorino & Caldwell (1976) at their lower Rayleigh numbers.

Turning to sequences of rolls at other values of $R$, we find that $\chi_m$ increases with increasing $R$. For instance, $\chi_m = 0{\cdot}30$, 0·33 and 0·37 when $R = 10^5$, $10^7$ and $10^9$ and $\lambda = 10$. Limited experiments with hexagons suggest a similar tendency. Thus we are left with a severe discrepancy: the evidence from the experiments of Marmorino & Caldwell (1976) is that $\chi$ decreases with increasing $R$, whereas our solutions behave conversely.

### 4.4. *The heat flux for steady convection*

In figure 5 is shown how the heat flux in the preferred type B solutions varies with $\lambda$ for several values of $R$. The heat flux is measured in units of its maximum value, which is achieved when salt is absent ($\lambda = 0$). For comparison the dashed curve denotes the heat flux $F$ in the experiments of Marmorino & Caldwell (1976), normalized in the manner of Turner (1965) by a presumed value of $F$ at $\lambda = 0$. It is not really clear whether the variation of $F$ with $\lambda$ is really the universal function represented by this curve (cf. Huppert 1971), since the range of $R$ in the laboratory experiments is not wide. Like the experimental values our numerical results are insensitive to $\lambda$ at large $\lambda$, though the values of the normalized heat fluxes are in disaccord. They also vary slowly with $R$.

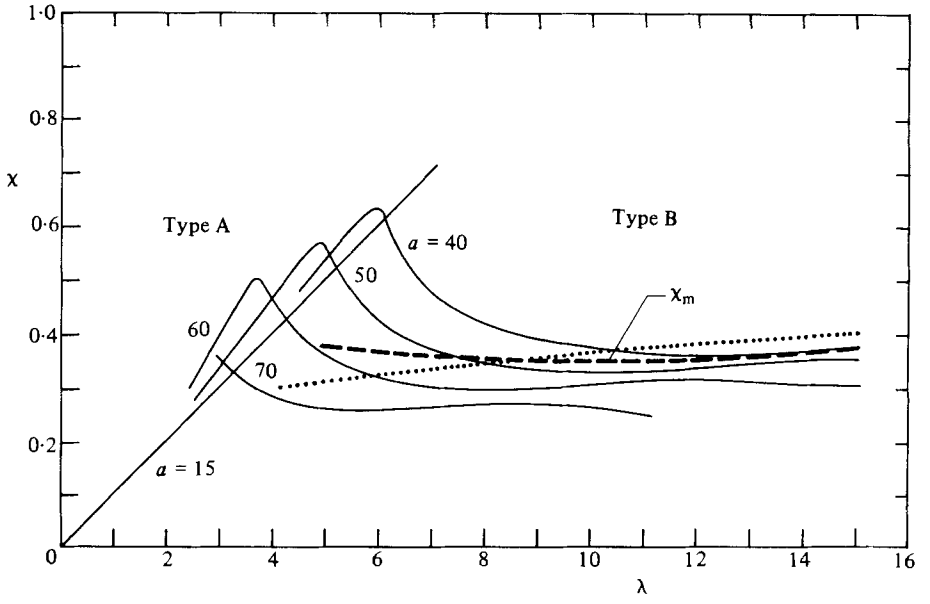


FIGURE 4. The flux ratio $\chi$ for rolls at $R = 10^8$ in a fluid with $\tau = 10^{-2}$ subject to free boundary conditions. The continuous lines are for the fixed wavenumbers indicated. They are all asymptotic to a straight line through the origin as $\lambda \to 0$, but we have truncated the curves to avoid crowding the diagram. The dashed line represents $\chi_m$; its value is 0·38 at $\lambda = 5$ (when $a_m = 58{\cdot}9$), decreases to 0·35 at $\lambda = 10$ ($a_m = 24{\cdot}7$) and returns to 0·38 at $\lambda = 15$ ($a_m = 21{\cdot}1$). The associated Nusselt number $N_m$ also hardly varies, being 36·5 at $\lambda = 5$, 38·0 at $\lambda = 10$ and 34·6 at $\lambda = 15$; in contrast the maximum $N$ at $\lambda = 0$ is 151. Our surveys at higher wavenumbers are too sparse to determine $\chi_m$ unambiguously when $\lambda < 5$. The dotted line is the value of $\chi_m$ evaluated from the asymptotic formulae (5.50) and (5.53) with $a = (\frac{1}{13}KR)^{\frac{1}{4}}$ and $k_2 = 2{\cdot}5$. Since the convective layers are symmetrical about their midplanes, $\lambda$ is equal to the effective stability parameter $\lambda_e$ that characterizes a single interface.

## 5. Asymptotic solutions for large $R$

The case of greatest interest to oceanography and astrophysics is that of very large $R$. Here we develop matched asymptotic expansions of the solutions in this limit. The main objective is to calculate the flux ratio $\chi$. The result is that $\chi = \lambda\tau^{\frac{1}{2}}$ when $\lambda$ is small, and that $\chi$ is insensitive to $\lambda$ when $\lambda$ is sufficiently large. In the latter case $\chi$ is given by (5.53) and (5.50), and is plotted in figure 5 for three values of $R$.

Solutions of types A and B have quite different structures, as can be seen from the numerical results. The interior equations are the only common feature, though it will be necessary to develop their solutions separately for the two cases. The type B solutions exist only when $\tau$ is small.

In the interior we introduce the scalings

$$W = W_0\Psi, \quad \Theta = NW_0^{-1}F, \quad \Phi = \mu NW_0^{-1}G, \quad \beta = NB, \quad \gamma = \mu N\Gamma, \tag{5.1}$$

where

$$W_0 = (NRa^2)^{\frac{1}{2}}, \tag{5.2}$$

which is large. In terms of the scaled variables, the modal equations (3.9)–(3.11), (3.14) and (3.15) become

$$(D^2-a^2)^2\Psi = F-\lambda\mu G, \tag{5.3}$$

$$W_0^{-2}(D^2-a^2)F = -B\Psi, \tag{5.4}$$

$$\tau W_0^{-2}(D^2-a^2)G = -\Gamma\Psi, \tag{5.5}$$

$$B+\Psi F = 1, \tag{5.6}$$

$$\Gamma+\tau^{-1}\Psi G = 1, \tag{5.7}$$

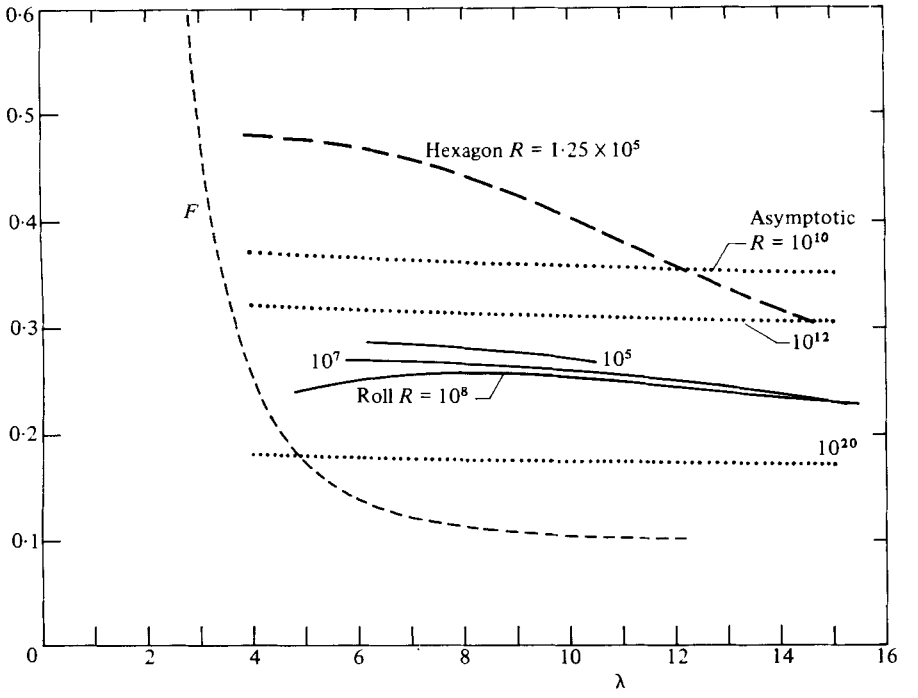


FIGURE 5. Dependence of the Nusselt number $N_m \equiv N(a_m)$, measured in units of its value at $\lambda = 0$, on the stability parameter $\lambda$. The continuous lines denote rolls at the Rayleigh numbers indicated and the dashed line hexagons for $\sigma = 6{\cdot}8$. All solutions are of type B, are subject to free boundary conditions and have $\tau = 10^{-2}$. For comparison is included the function $F = 0{\cdot}101 \exp\{4{\cdot}6 \exp[-0{\cdot}54(\lambda - 1)]\}$, which, according to Marmorino & Caldwell (1976), is a good fit to their experimental data. The dotted curves are asymptotic results, obtained from the analysis of §5. Numerical solution at $a = a_m$ are not available for $\lambda$ in the range in which the transition between the type A and type B interfaces occurs, but it is apparent from figure 4 that as $\lambda$ decreases $N_m$ must first rise rapidly near $\lambda = 3$ to about 0·85, the value for type A solutions, and then it increases gradually to unity as $\lambda$ decreases to zero.

which must be solved subject to the constraints

$$\int_0^1 B\,dz = N^{-1}, \tag{5.8}$$

$$\int_0^1 \Gamma dz = (\mu N)^{-1} \tag{5.9}$$

and appropriate boundary conditions. It will become evident that the boundary conditions that must be applied depend on $\lambda$.

The solutions are considered to be expanded in an asymptotic sequence as follows:

$$\Psi = \Psi_0 + W_0^{-2}\Psi_1 + \ldots . \tag{5.10}$$

In leading order it follows from (5.4) and (5.5) that $B_0 = 0$, $\Gamma_0 = 0$; whence $F_0 = \Psi_0^{-1}$ and $G_0 = \tau\Psi_0^{-1}$. The momentum equation (5.3) then becomes

$$\Psi_0(D^2 - a^2)^2\Psi_0 = 1 - \chi \equiv K. \tag{5.11}$$

It should be observed that the scaling $\tilde{\Psi}_0 = K^{-\frac{1}{2}}\Psi_0$ reduces the interior equation to that obtained in the absence of the salinity field.

### 5.1. *Type A solutions: $\lambda$ small*

In this case the stabilizing effect of the salinity field is insufficient to alter the functional form of the velocity. It merely reduces the amplitude. The problem of determining the velocity field is then analogous to that of Bénard convection with free boundaries, and has been discussed by Howard (1965). Equation (5.11) must be solved subject to the conditions $\Psi_0 = 0$, $D^2\Psi_0 = 0$ at $z = 0, 1$. Near $z = 0$ the solution has the form

$$\Psi_0 = K^{\frac{1}{2}}\left[Az + \frac{1}{6A}z^3 \ln z + \ldots\right], \tag{5.12}$$

where $A$ is a constant that is fixed by the condition that the solution also satisfies the boundary conditions at $z = 1$. Howard (1965) gives $Aa = 0{\cdot}836$ at the wavenumber $a_m$ that maximizes the heat flux; Van der Borght, Murphy & Spiegel (1972) and Gough *et al.* (1975*a*) give a very approximate expression for $A$ for any $a$ in the vicinity of $a_m$.

5.1.1. *The boundary layer.* The boundary-layer equations are obtained by setting $z = \epsilon\eta$, where $\epsilon$ is the boundary-layer thickness, and by introducing the new dependent variables $\psi(\eta)$, $f(\eta)$ and $g(\eta)$ defined by

$$\Psi = \epsilon K^{\frac{1}{2}} A\psi, \quad F = \epsilon^{-1}K^{-\frac{1}{2}}A^{-1}f, \quad G = \tau\epsilon^{-1}K^{-\frac{1}{2}}A^{-1}g. \tag{5.13}$$

Equations (5.3)–(5.7) then become

$$\Psi^{\mathrm{iv}} = O(\epsilon^2), \tag{5.14}$$

$$f'' = -W_0^2\epsilon^4 KA^2 B\psi + O(\epsilon^2), \tag{5.15}$$

$$g'' = -W_0^2\epsilon^4 KA^2\tau^{-2}\Gamma\psi + O(\epsilon^2), \tag{5.16}$$

$$B + \psi f = 1, \tag{5.17}$$

$$\Gamma + \psi g = 1, \tag{5.18}$$

where a prime denotes differentiation of a function with respect to its argument. It is evident that one must set

$$W_0^2\epsilon^4 KA^2 = 1. \tag{5.19}$$

The boundary conditions at $\eta = 0$ are $\psi = 0$, $\psi'' = 0$, $f = 0$ and $g = 0$. As $\eta \to \infty$ the solutions must match the interior solution which, expressed in boundary-layer variables to leading order in $\epsilon$, is

$$\psi \sim \eta, \quad f \sim \eta^{-1}, \quad g \sim \eta^{-1}. \tag{5.20}$$

The equations for $\psi$ and $f$ are precisely those encountered in the absence of salinity and have solutions, to leading order in $\epsilon$:

$$\psi = \eta, \tag{5.21}$$

$$f = 2^{-\frac{3}{4}}\eta^{\frac{1}{2}}\left\{K_{\frac{1}{4}}(\tfrac{1}{2}\eta^2)\int_0^{\frac{1}{2}\eta^2} y^{\frac{1}{4}}I_{\frac{1}{4}}(y)\,dy + I_{\frac{1}{4}}(\tfrac{1}{2}\eta^2)\int_{\frac{1}{2}\eta^2}^{\infty} y^{\frac{1}{4}}K_{\frac{1}{4}}(y)\,dy\right\}, \tag{5.22}$$

where $I_{\frac{1}{4}}$ and $K_{\frac{1}{4}}$ are modified Bessel functions of the first and second kinds. The solution for $g$ may now be obtained immediately by noticing that the scaling $\eta = \tau^{\frac{1}{2}}\xi$, $g = \tau^{-\frac{1}{2}}h$ transforms the problem into that which determined $f$. Thus

$$g(\eta) = \tau^{-\frac{1}{2}}f(\tau^{-\frac{1}{2}}\eta). \tag{5.23}$$

5.1.2. *The heat and salinity fluxes.* The fluxes $N$ and $\mu N$ are determined from the constants (5.8) and (5.9). With the help of (5.6), (5.8) may be written

$$N^{-1} = \int_0^1 (1 - \Psi F)\, dz. \tag{5.24}$$

The contribution to the integral from the interior is $O(W_0^{-2})$, which is small compared with $N^{-1}$: the boundary-layer contribution is

$$2\epsilon \int_0^\infty (1 - \psi f)\, d\eta \equiv 2\epsilon k, \tag{5.25}$$

and $k = 2^{-\frac{1}{2}}[\Gamma(\frac{3}{4})]^2 = 1{\cdot}06$, as was found by Howard (1965). Here $\Gamma$ is the gamma function. The factor 2 arises because there are two boundary layers in the domain, or two sides to the boundary layer in the case of a full diffusive interface. Thus $N \sim 1/2\epsilon k$, which yields, with the help of (5.2) and (5.19),

$$N \sim \left[\frac{KR(Aa)^2}{(2k)^4}\right]^{\frac{1}{3}} \quad \text{as} \quad R \to \infty. \tag{5.26}$$

The constraint (5.9) can be treated similarly, giving

$$\mu N \sim \tau^{-\frac{1}{2}}\left[\frac{KR(Aa)^2}{(2k)^4}\right]^{\frac{1}{3}} \quad \text{as} \quad R \to \infty. \tag{5.27}$$

Thus $\mu \sim \tau^{\frac{1}{2}}$, and the buoyancy-flux ratio is

$$\chi = \lambda\mu\tau \sim \lambda\tau^{\frac{1}{2}} \quad \text{as} \quad R \to \infty.$$

This result can be obtained also for $C \neq 0$, and it agrees with numerical results such as those depicted in figures 3 and 4 when $\lambda$ is small.

### 5.2. *Type B solutions*

Solutions of this class occur when $\tau$ is small enough to produce a thin haline boundary layer within the thermal boundary layer, and $\lambda$ is large enough that significant stabilization of the flow occurs within the haline boundary layer. In solutions of type A the haline boundary-layer thickness is $\tau^{\frac{1}{2}}$ times that of the thermal boundary layer. According to the numerical results, typified by the hexagonal solutions in figure 1, the haline boundary layer expands as $\lambda$ increases (in the domain of the type B solutions). In this section an asymptotic solution will be sought in which the haline boundary layer is still thin compared with the thermal layer. Thus we must expect that the solution might cease to be valid if $\lambda$ assumes sufficiently high values. Perusal of the numerical results reveals that, although $W$ varies linearly with $z$ very close to the boundaries, its dependence on $z$ is quadratic throughout most of the thermal boundary layer. Thus the haline boundary layer is a region where the velocity is greatly reduced, and on the thermal lengthscale or greater it appears as a rigid boundary.

Guided by these remarks we seek the solution of the interior equation (5.11) satisfying $\Psi_0 = 0$, $D\Psi_0 = 0$ at $z = 0, 1$. This is essentially the problem considered by Stewartson (1966) in a discussion of thermal convection between rigid boundaries. We recall that, whereas in the free-boundary case $N$ is maximized with respect to $a$ when $a = O(1)$, for thermal convection between rigid boundaries $N$ is maximized when $a = O(R^{\frac{1}{4}})$. Thus we allow the possibility that $a$ be large, which produces boundary layers in the interior solution of thickness $a^{-1}$. The analysis will be valid when $a$ is less than or of the order of the maximizing value, and then $a^{-1}$ is greater than the

thermal boundary-layer thickness. Except in the boundary layers the interior solution is asymptotically constant with $\Psi_0 \sim a^{-2}K^{-\frac{1}{2}}$, $B_1 \sim a^6K^{-1}$ and $\Gamma_1 \sim \tau^2a^6K^{-1}$, and as Stewartson has shown, has the property

$$\Psi_0 \sim K^{\frac{1}{2}}z^2\left(\ln\frac{1}{az}\right)^{\frac{1}{2}} \quad \text{as} \quad az \to 0. \tag{5.28}$$

5.2.1. *The thermal boundary layer.* The analysis is analogous to Stewartson's discussion of thermal convection. Setting $z = \epsilon\eta$, where $\epsilon$ is the thermal boundary-layer thickness defined by

$$\epsilon^6 \ln\frac{1}{a\epsilon} = K^{-1}W_0^{-2}, \tag{5.29}$$

and introducing new dependent variables according to

$$\Psi = K^{\frac{1}{2}}\epsilon^2\left(\ln\frac{1}{a\epsilon}\right)^{\frac{1}{2}}\psi, \quad F = K^{-\frac{1}{2}}\epsilon^{-2}\left(\ln\frac{1}{a\epsilon}\right)^{\frac{1}{2}}f, \quad G = \tau K^{-\frac{1}{2}}\epsilon^{-2}\left(\ln\frac{1}{a\epsilon}\right)^{-\frac{1}{2}}g, \tag{5.30}$$

the boundary-layer equations, to leading order in powers of $\epsilon$, become

$$\psi^{\mathrm{iv}} - K^{-1}\left(\ln\frac{1}{a\epsilon}\right)^{-1}(f - \chi g) = 0, \tag{5.31}$$

$$f'' + \psi(1 - \psi f) = 0, \tag{5.32}$$

$$g'' + \tau^{-2}\psi(1 - \psi g) = 0. \tag{5.33}$$

In anticipation of the haline boundary layer, these equations are to be solved subject to the conditions that $\psi = 0$, $\psi' = 0$, $f = 0$ at $\eta = 0$, and that the solutions match the interior equation as $\eta \to \infty$, namely

$$\psi \sim \eta^2, \quad \phi \sim \eta^{-2}, \quad g \sim \eta^{-2} \quad \text{as} \quad \eta \to \infty. \tag{5.34}$$

The balance $g\psi \sim 1$ is maintained throughout this boundary layer. The thermal part of the problem is just that studied by Stewartson:

$$\psi = \eta^2; \tag{5.35}$$

$f$ can be expressed as integrals of modified Bessel functions, and has the property

$$f \sim 2H\eta \quad \text{as} \quad \eta \to 0, \tag{5.36}$$

where

$$H = 2^{-\frac{1}{6}}[\Gamma(\tfrac{1}{6})]^{-1}\int_0^\infty y^{\frac{1}{6}}K_{\frac{1}{6}}(y)\,dy.$$

Recalling that $\tau$ is small, the salinity fluctuation can be expanded in powers of $\tau^2$ to give

$$g = \eta^{-2} + 6\tau^2\eta^{-8} + \ldots. \tag{5.37}$$

It can be shown that the second term matches the $O(W_0^{-2})$ term of the interior solution when expressed in thermal boundary-layer variables.

5.2.2. *The haline boundary layer.* The scaling in the haline boundary layer depends on the matching with the thermal layer. To determine this it is convenient to introduce a scaling factor $\delta$ defined in terms of a parameter $\alpha$, to be specified later, according to

$$\delta = \tau^{\frac{1}{3}}\left(\alpha K\chi^{-1}\ln\frac{1}{a\epsilon}\right)^{\frac{1}{6}}. \tag{5.38}$$

In terms of a boundary-layer coordinate $\xi = \delta^{-1}\eta$ and the dependent variables $u(\xi)$, $v(\xi)$ and $w(\xi)$ defined by

$$\psi = \tau\delta^{-1}u, \quad f = \delta v, \quad g = \tau^{-1}\delta w, \tag{5.39}$$

(5.31)–(5.33) become

$$u^{\mathrm{iv}}+\alpha(w-\tau\chi^{-1}v)=0, \tag{5.40}$$

$$v''+\tau u(1-\tau uv)=0, \tag{5.41}$$

$$w''+u(1-uw)=0. \tag{5.42}$$

The boundary conditions to be satisfied at $\xi=0$ are that $u$, $v$, $w$ and $u''$ vanish. To leading order in $\tau$ (5.41) is $v''=0$, which has the solution $v=2H\xi$ matching the asymptotic form (5.36) of the solution in the thermal boundary layer. Provided that $\tau\chi^{-1}\ll 1$, the buoyancy term in brackets in the momentum equation (5.40) is now dominated by the salinity fluctuation and this impedes the flow, whereas in the interior it is the temperature fluctuation that is more important. Equations (5.40) and (5.42) may be combined to give

$$u^{\mathrm{vi}}-u^2u^{\mathrm{iv}}-\alpha u\approx 0. \tag{5.43}$$

We have not solved this equation, but we note that it admits solutions of the form

$$u\sim\alpha^{\frac{1}{2}}\xi^2(\ln\xi)^2[1+C_1+\tfrac{1}{8}(\ln\xi)^{-1}\ln\ln\xi+C_2\ln\xi+\ldots] \quad \text{as} \quad \xi\to\infty, \tag{5.44}$$

where $C_1$ and $C_2$ are constants. The form of the salinity fluctuation can then be obtained from (5.40):

$$\begin{aligned} w\sim{}&\alpha^{-\frac{1}{2}}\xi^{-2}(\ln\xi)^{-\frac{1}{2}}[1-C_1-\tfrac{1}{8}(\ln\xi)^{-1}\ln\ln\xi+\ldots]\\ &+6\alpha^{-\frac{3}{2}}\xi^{-8}(\ln\xi)^{-\frac{3}{2}}[1-C_1-\tfrac{3}{8}(\ln\xi)^{-1}\ln\ln\xi+\ldots] \quad \text{as} \quad \xi\to\infty. \end{aligned} \tag{5.45}$$

Expressed in thermal boundary-layer variables (5.44) becomes

$$\psi\sim\left(\frac{\chi\ln(1/\delta)}{K\ln(1/a\epsilon)}\right)^{\frac{1}{2}}\eta^2\left[1+C_1+\frac{1}{8}\left(\ln\frac{1}{\delta}\right)^{-1}\ln\ln\frac{1}{\delta}+\left(\ln\frac{1}{\delta}\right)^{-1}(C_2+\tfrac{1}{2}\ln\eta)+\ldots,\right. \tag{5.46}$$

whose leading term matches (5.35) provided that

$$\ln\frac{1}{\delta}=K\chi^{-1}\ln\frac{1}{a\epsilon}, \tag{5.47}$$

which, together with (5.38), determines $\alpha$. The leading terms of the expansion of (5.45) in thermal boundary-layer variables then match (5.37). Moreover, it can be shown that the condition (5.47), together with the choices

$$C_1=-\tfrac{1}{8}(1+K^{-1}\chi)\left(\ln\frac{1}{a\epsilon}\right)^{-1}\ln\ln\frac{1}{a\epsilon},$$

and $C_2=0$, enables the other terms in (5.46) to be matched to terms in the thermal boundary-layer solution generated by considering higher orders in the asymptotic expansions of $\psi$ and $\Psi$.

5.2.3. *The heat and salinity fluxes.* As before, the Nusselt number is determined from the constraint (5.8). Thus

$$\begin{aligned} N^{-1}&\sim W_0^{-2}\int_0^1 B_1\,dz+2\epsilon\int_0^\infty(1-\psi f)\,d\eta+2\epsilon\delta\int_0^\infty(1-uv)\,d\xi\\ &\sim W_0^{-2}a^6K^{-1}+2\epsilon k_1, \end{aligned} \tag{5.48}$$

where

$$k_1\equiv\int_0^\infty(1-\psi f)\,d\eta=(\tfrac{2}{9})^{\frac{1}{3}}[\Gamma(\tfrac{2}{3})]^2=1{\cdot}11 \tag{5.49}$$

(Stewartson 1966). The contributions from the $a^{-1}$ boundary layers and the haline boundary layers are small compared with the terms retained. Substituting for $W_0$ from

(5.2) then gives $N^{-1}(1-a^4/KR) \sim 2\epsilon k_1$, which yields, after eliminating $\epsilon$ using (5.29) and (5.2),

$$N \sim \left(1-\frac{a^4}{KR}\right)^{\frac{6}{5}}\left\{\frac{KRa^2}{5(2k_1)^6}\ln\left[KRa^{-3}\left(1-\frac{a^4}{KR}\right)\right]\right\}^{\frac{1}{5}} \quad \text{as} \quad R\to\infty. \tag{5.50}$$

Similarly the constraint (5.9) gives

$$\begin{aligned}\mu^{-1}N^{-1} &\sim W_0^{-2}\int_0^1 \Gamma_1\,dz + O(\epsilon\tau^2) + 2\epsilon\delta\int_0^\infty (1-uw)\,d\xi \\ &\sim W_0^{-2}\tau^2a^2K^{-1} + 2\epsilon\delta k_2,\end{aligned} \tag{5.51}$$

where

$$k_2 \equiv \int_0^\infty (1-uw)\,d\xi \tag{5.52}$$

is a constant of order unity. The $O(\epsilon\tau^2)$ term is the contribution from the thermal boundary layer; it is small compared with the contribution from the haline boundary layer, though this must be confirmed *a posteriori*. The contribution from the interior is also small for $a$ in the range considered here. Thus $\mu^{-1}N^{-1} \sim 2\epsilon\delta k_2$; it can now be divided into (5.48) to obtain an expression for $\mu$ from which $\delta$ can be eliminated using (5.47) and the relation between $\epsilon$ and $N$. There results a transcendental equation for $\chi$:

$$\chi \sim \frac{\lambda\tau}{k_2}\left\{k_1\left[1-\frac{a^4}{(1-\chi)R}\right]^{-1}\left(\frac{2N}{a}\right)^{1-\chi}\right\}^{1/\chi}, \tag{5.53}$$

with $N$ given by (5.50).

It is not easy to solve (5.43) numerically subject to the requisite boundary and matching conditions, because the solutions are very sensitive to conditions at large $\xi$. Therefore, since the solution of (5.53) for $\chi$ depends only weakly on the constant $k_2$, we have not determined $k_2$. Nevertheless, we find that setting $k_2 \approx 2{\cdot}5$ yields values of $\chi$ within about 10 % of the numerical values for $R$ in the range $[10^7, 10^9]$ over a wide range of $a$. The limit (5.50) can overestimate the numerical results by about 50 %, though it should be borne in mind that since the asymptotic analysis requires $\ln R$ to be large the numerical results can hardly be expected to be in the asymptotic regime. In contrast, at $R = 10^9$ Stewartson's (1966) formula for $N$ of Bénard convection, which is simply (5.50) with $K = 1$, overestimates numerical solutions by only about 20 %; at $R = 10^{20}$ and $a = 1$, by 5 %.

The value of $\chi$ implied by (5.53) and (5.50) exhibits the qualitative features of the numerical results: it decreases with increasing $a$, and increases only gradually with increasing $\lambda$ and with $\tau$. Moreover, it also increases with $R$, and approaches unity as $R\to\infty$. This behaviour is illustrated in figures 4 and 5, where the asymptotic solutions are compared with the numerical results: it is evident from (5.50) that the normalized heat fluxes plotted in figure 5 reflect the value of $\chi$. The wavenumber $a_m \sim (\frac{1}{13}KR)^{\frac{1}{4}}$ at which the buoyancy flux $KN$ is maximized decreases slowly with $\lambda$. The Nusselt number $N$ is maximized at the same value of $a$, to this order of accuracy. Equations (5.53) and (5.50) can be solved for $\chi$. When $a \approx a_m$ the result is

$$K = 1-\chi \sim 20\ln\left(\frac{k_2}{\lambda\tau}\right)(\ln R)^{-1} \quad \text{as} \quad R\to\infty. \tag{5.54}$$

It then follows from (5.47) that $\delta \sim \lambda\tau$, which justifies the neglect of the term $O(\epsilon\tau^2)$ in (5.51). It should be noted also that the proviso $\tau\chi^{-1} \ll 1$ made in deriving (5.43) is also satisfied. The approach $\chi\to 1$ is slow: for example when $R = 10^{20}$ and $a = 5\times 10^4$, the value at about which $KN$ is maximized, (5.50) and (5.53) give $\chi \approx 0{\cdot}58$. Even this value of $R$ is not large enough for (5.54) to be applicable.

### 5.3. *The buoyancy-flux ratio*

When $\lambda$ is small, salinity is of little consequence. A haline boundary layer is set up within the interface, but it is too weak to divert the flow. The result of transporting salt through the layer is simply to reduce buoyancy by a factor $1-\chi$, and hence to modify the velocity field to that encountered in ordinary thermal convection at a Rayleigh number $(1-\chi)R$. The structures of the haline and thermal boundary layers are similar, save that the haline layer is thinner by a factor $\tau^{\frac{1}{2}}$. Consequently the salinity flux $\mu N$, measured in units of the diffusive value, is $\tau^{-\frac{1}{2}}N$, where $N$ is the Nusselt number. The flux ratio $\chi = \lambda\mu\tau$ is thus $\tau^{\frac{1}{2}}\lambda$, which increases linearly with $\lambda$. This is the type A solution.

A solution of this form cannot persist to arbitrarily large $\lambda$ since the flow would be entirely suppressed once $\chi$ attained unity. Indeed, at values of $\lambda$ considerably below $\tau^{-\frac{1}{2}}$, penetration of the flow into the haline boundary layer is impeded by the stable stratification; even horizontal motion within this boundary layer is inhibited because the fluid would eventually be forced away from the interface and become negatively buoyant. Thus, to the fluid outside, the haline boundary layer appears as a rigid boundary, even though no no-slip condition is imposed within the interface. This is the type B solution. In this case too the flow in the interior resembles that of ordinary thermal convection at a Rayleigh number of $(1-\chi)R$, but with rigid boundaries. Thus, provided that $\chi$ is not too close to unity, the heat flux is insensitive to $\lambda$. At the edge of the haline boundary layer diffusion is balanced by advection from or into the main body of the adjacent convecting layer. The velocity amplitude in the interior flow, which like $N$ varies only weakly with $\lambda$ at constant $R$, thus fixes the salinity gradient in the boundary layer and hence the salinity flux. Therefore $\mu N$ is approximately proportional to $\lambda^{-1}$, and $\chi = \lambda\mu\tau$ is independent of $\lambda$. A further consequence of this balance is that the haline boundary-layer thickness increases almost linearly with $\lambda$. Clearly if $\lambda$ were very large the asymptotic analysis in §5.2 would no longer be valid, since it assumes the haline boundary layer to remain thin compared with the thermal layer. Nevertheless, the argument here suggests that even then the buoyancy-flux ratio would remain insensitive to the stability parameter.

The transition between the two kinds of flow as $\lambda$ is increased produces a sharp decline in the Nusselt number, essentially from free-boundary to rigid-boundary values for ordinary convection at the appropriate values $(1-\chi)R$ of the Rayleigh number. This is evident in plots of $N$ against $\lambda$ at fixed $R$ and $a$, which we have not displayed here. This feature is seen too in the experimental data, but quantitative agreement between theory and experiment has not been achieved.

## 6. Discussion

The principal result of this investigation is that the single-mode representation of a diffusive thermohaline interface reproduces the near constancy of the buoyancy-flux ratio $\chi$ as the density ratio $\lambda$ is varied. This occurs only when $\tau$ is small and $\lambda$ is sufficiently large, and is a common feature of all our solutions with wavenumbers comparable to that which maximizes the buoyancy flux. The interface, which we have labelled as being of type B, may be regarded as a pair of nested diffusive boundary layers: the ratio of the thicknesses of the inner haline layer and the thermal layer increases linearly with $\lambda$, and the structure of the haline layer becomes more complicated as $\lambda$ increases, developing weak viscously driven countercells.

The type B boundary-layer structure bears a superficial resemblance to that

assumed in the recent kinematical argument presented by Linden & Shirtcliffe (1978). These authors suppose that a permanent diffusive layer is embedded in a broader boundary layer which is intermittently ablated, in much the same way that Howard (1966) proposed in his theory of thermal convection at high Rayleigh numbers. Heat and salt perturbations diffuse from the inner layer until the stratification becomes unstable. Then a burst of mixing is presumed to ensue, which homogenizes the convective layers. At the crux of the argument is the assumption that the fluid motion extends only to the level at which the density is equal to that in the middle of the convective layer. At this level the contributions to the density anomalies from heat and salt are equal in magnitude. The ratio of the quantities of heat and salt that have diffused beyond that level into the region that suffers ablation is therefore proportional to only the ratio of the square roots of the corresponding diffusivities. It follows immediately that $\chi = \tau^{\frac{1}{2}}$, irrespective of $R$ and $\lambda$. Our attempt at modelling the dynamics has predicted that the flow actually penetrates into the stably stratified layer further than Linden & Shirtcliffe assume, by an amount which increases with increasing $R$. We find, therefore, that the salt flux is preferentially enhanced, and that $\chi$ increases slowly with $R$.

Another consequence of Linden & Shirtcliffe's assumptions is that the heat and salt fluxes contain the factor $1-\tau^{\frac{1}{2}}\lambda$, as do our type A solutions at low $\lambda$. Presumably this results from the assumption that the ablation process is similar for salt and heat. Thus the model predicts that the fluxes vanish when $\lambda$ exceeds $\tau^{-\frac{1}{2}}$, just as would have been the case for our type A solutions had the structure of the velocity field not changed to that of type B as $\lambda$ increased. Thus although Linden & Shirtcliffe have succeeded in constructing a flux ratio that appears to agree with some of the experiments, their model is unable to explain why convection is sustained at the higher values of the stability parameter under which experiments have been performed.

The model presented in this paper is incomplete too, particularly because the single-mode representation contains the undetermined wavenumber $a$. In the case of thermal convection between rigid boundaries, the experimental Nusselt numbers can be reproduced by the single-mode mean-field approximation with a value of $a$ similar to though somewhat different from the maximizing value (cf. II). We have been tempted to make such a choice in this study, though whether it is preferable to think in terms of the wavenumber $a_{\mathrm{m}}$ that maximizes the buoyancy flux or that which maximizes the Nusselt number is unclear. In any case, when $R$ is large the single-mode representation discussed in this paper predicts that the two are nearly equal. However, if one adopts such a choice, the predicted dependence of the buoyancy-flux ratio $\chi$ on $R$ disagrees with experiment: Marmorino & Caldwell (1976) found that $\chi$ appears to decrease with $R$, whereas the theory implies that it increases and approaches unity as $R$ tends to infinity, at least when $C = 0$.

As in I, our motivation for this study was the desire to find a tractable model that can be applied to natural flows, where the values of $R$, $\sigma$, and possibly $\tau$, are at present inaccessible to either controlled experiment or direct numerical integration of the equations of motion. Aside from the obvious applications to oceanography, diffusive interfaces may play an important role in determining the transport of helium and other products of nuclear reactions from the cores of evolved stars. If layering takes place on a small scale at the edges of stellar cores, the Boussinesq approximation would be applicable and one would not be faced with the complexities of compressibility normally encountered in stellar convection zones. One might then have some confidence in a theory tested by laboratory experiment and extrapolated to conditions relevant to stars. Experiments by Turner (1965) and Shirtcliffe (1973) (see also Turner

1973) have suggested that $\chi = \tau^{\frac{1}{2}}$. This would be a particularly attractive result, if verified, because it is independent of $R$, and hence of the detailed structure of the environment. Though Marmorino & Caldwell's recent experiments have revealed a Rayleigh-number dependence, the limit $\chi \sim \tau^{\frac{1}{2}}$ as $R \to \infty$ is not inconsistent with their results. However, this result has yet no theoretical backing, and the possibilities either that $\chi \to 0$ as $R \to \infty$ or that $\chi$ tends to a limit considerably in excess of $\tau^{\frac{1}{2}}$ when $\tau$ is extremely small are not ruled out by experiment. It is essential to understand what controls $\chi$ at very high Rayleigh numbers (and low Prandtl numbers) before the interior of evolved stars can be modelled, and further experiments at higher $R$ would help considerably.

Whatever the behaviour of $\chi$ as $R \to \infty$, it is important to know whether it depends on the Prandtl number $\sigma$. In thermal convection it is known that $N$ is insensitive to $\sigma$ when $\sigma \gtrsim 1$, but there is evidence that $N$ is reduced significantly when $\sigma \ll 1$ (Spiegel 1962, 1971). It is not unlikely that the salinity and heat fluxes scale differently with Prandtl number, so $\chi$ might be substantially different at the very low Prandtl numbers encountered in stars. Though the single-mode equations with $C \neq 0$ do contain $\sigma$, in view of their failure to reproduce Marmorino & Caldwell's results we have not attempted to determine the Prandtl-number dependence of the type B solutions.

The observed Rayleigh-number dependence of $\chi$ might be reproduced by a single-mode analysis if $a$ were chosen to increase faster than $a_{\mathrm{m}}$. However this does not reproduce isothermal, isohaline convective regions on either side of the interface. What may be necessary is a multimode analysis, though with a very limited number of modes one is still faced with the problem of deciding which wavenumbers to select (Toomre, Gough & Spiegel 1982). It may be possible to choose them so as to reproduce experimental results, but one runs the risk of being left with no confirmable prediction with which to test the theory. Nevertheless one does observe in the laboratory horizontal scales of motion comparable to both the depth of the convecting layers and to the thickness of the interface, so perhaps it should not be expeeted that modelling with a single wavenumber could be successful.

Finally it must be realized that the phenomenon may be essentially time dependent, and that no number of steady modes can faithfully reproduce even the time-averaged structure of the interface. If intermittent ablation is an important process, as Linden (1974) has suggested, it may be necessary to produce a much more elaborate model before one can extrapolate with confidence to convection in natural circumstances.

We thank D. R. Caldwell, R. W. Griffiths, H. E. Huppert, P. F. Linden, G. O. Marmorino, E. A. Spiegel and J. S. Turner for interesting conversations concerning the subject matter of this paper, and H. E. Huppert for reading and commenting on the original version of this paper. This research was supported in part by the National Science Foundation Physical Oceanography Program through Grant DES74-14439, by the Advanced Studies Program of the National Center for Atmospheric Research, by the National Aeronautics and Space Administration through Grant NSG-7511, and by the Science Research Council. Computing facilities were provided by the Goddard Institute for Space Studies in New York, by the Institute of Theoretical Astronomy in Cambridge, and by the National Center for Atmospheric Research in Boulder.

The Joint Institute for Laboratory Astrophysics is supported jointly by the University of Colorado and the National Bureau of Standards.

## REFERENCES


BAINES, P. G. & GILL, A. E. 1969 On thermohaline convection with linear gradients. *J. Fluid Mech.* **37**, 289–306.

BROUGHTON, J. M. 1972 Experiments on steady layered convection in a doubly-diffusive system. M.S. thesis, Colorado State University.

CRAPPER, P. F. 1973 An experimental study of mixing across density interfaces. Ph.D. thesis, University of Cambridge.

CRAPPER, P. F. 1975 Measurements across a diffusive interface. *Deep-Sea Res.* **22**, 537–545.

GOUGH, D. O., SPIEGEL, E. A. & TOOMRE, J. 1975*a* Modal equations for cellular convection. *J. Fluid Mech.* **68**, 695–719.

GOUGH, D. O., SPIEGEL, E. A. & TOOMRE, J. 1975*b* Highly stretched meshes as functionals of solutions. In *Proc. 4th Int. Conf. Numer. Methods Fluid Mech.* (ed. R. D. Richtmyer). *Lecture Notes in Physics*, vol. 35, pp. 191–196. Springer.

GRIFFITHS, R. W. 1979*a* Transport through thermohaline interfaces in a viscous fluid and a porous medium. Ph.D. thesis, Australian National University.

GRIFFITHS, R. W. 1979*b* The transport of multiple components through thermohaline diffusive interfaces. *Deep-Sea Res.* **26**A, 383–397.

HERRING, J. R. 1963 Investigations of problems in thermal convection. *J. Atmos. Sci.* **20**, 325–338.

HERRING, J. R. 1964 Investigation of problems in thermal convection: rigid boundaries. *J. Atmos. Sci.* **21**, 277–290.

HOWARD, L. N. 1965 Boundary layer treatment of the mean field equations. *Woods Hole Oceanographic Inst. GFD Notes* no. 65–51, vol. I, pp. 124–126.

HOWARD, L. N. 1966 Convection at high Rayleigh number. In *Proc. 11th Int. Cong. Appl. Mech.* (ed. H. Görtler), pp. 1109–1115. Springer.

HUPPERT, H. E. 1971 On the stability of a series of double-diffusive layers. *Deep-Sea Res.* **18**, 1005–1021.

HUPPERT, H. E. & LINDEN, P. F. 1979 On heating a stable salinity gradient from below. *J. Fluid Mech.* **95**, 431–464.

HUPPERT, H. E. & MOORE, D. R. 1976 Nonlinear double-diffusive convection. *J. Fluid Mech.* **78**, 821–854.

LINDEN, P. F. 1973 The interaction of a vortex ring with a sharp density interface: a model for turbulent entrainment. *J. Fluid Mech.* **60**, 467–480.

LINDEN, P. F. 1974 A note on the transport across a diffusive interface. *Deep-Sea Res.* **21**, 283–287.

LINDEN, P. F. 1976 The formation and destruction of fine-structure by double-diffusive processes. *Deep-Sea Res.* **23**, 895–908.

LINDEN, P. F. & SHIRTCLIFFE, T. G. L. 1978 The diffusive interface in double-diffusive convection. *J. Fluid Mech.* **87**, 417–432.

MARMORINO, G. O. 1974 Equilibrium heat and salt transport through a diffusive, thermohaline interface. M.S. thesis, Oregon State University.

MARMORINO, G. O. & CALDWELL, D. R. 1976 Equilibrium heat and salt transport through a diffusive thermohaline interface. *Deep-Sea Res.* **23**, 59–67.

ROBERTS, P. H. 1966 On non-linear Bénard convection. In *Non-Equilibrium Thermodynamics, Variational Techniques, and Stability* (ed. R. Donnelly, R. Hermann & I. Prigogine), pp. 125–162. University of Chicago Press.

SHIRTCLIFFE, T. G. L. 1973 Transport and profile measurements of the diffusive interface in double diffusive convection with similar diffusivities. *J. Fluid Mech.* **57**, 27–43.

SPIEGEL, E. A. 1962 Thermal turbulence at very small Prandtl number. *J. Geophys. Res.* **67**, 3063–3070.

SPIEGEL, E. A. 1971 Convection in stars. I. Basic Boussinesq convection. *Ann. Rev. Astron. Astrophys.* **9**, 323–352.

STERN, M. E. 1960 The 'salt fountain' and thermohaline convection. *Tellus* **12**, 172–175.

STEWARTSON, K. 1966 Asymptotic theory in limit $R \to \infty$. In *Non-Equilibrium Thermodynamics, Variational Techniques, and Stability* (ed. R. Donnelly, R. Hermann & I. Prigogine), pp. 158–162. University of Chicago Press.

TOOMRE, J., GOUGH, D. O. & SPIEGEL, E. A. 1977 Numerical solutions of single-mode convection equations. *J. Fluid Mech.* **79**, 1–31.

TOOMRE, J., GOUGH, D. O. & SPIEGEL, E. A. 1982 Time-dependent solutions of multimode convection equations. *J. Fluid Mech.* **125**, 99–122.

TURNER, J. S. 1965 The coupled turbulent transports of salt and heat across a sharp density interface. *Int. J. Heat Mass Transfer* **8**, 759–767.

TURNER, J. S. 1968 The behaviour of a stable salinity gradient heated from below. *J. Fluid Mech.* **33**, 183–200.

TURNER, J. S. 1973 *Buoyancy Effects in Fluids.* Cambridge University Press.

TURNER, J. S. & STOMMEL, H. 1964 A new case of convection in the presence of combined vertical salinity and temperature gradients. *Proc. Natl Acad. Sci.* **52**, 49–53.

VAN DER BORGHT, R., MURPHY, J. O. & SPIEGEL, E. A. 1972 On magnetic inhibition of thermal convection. *Aust. J. Phys.* **25**, 703–718.

VERONIS, G. 1965 On finite amplitude instability in thermohaline convection. *J. Mar. Res.* **23**, 1–17.

VERONIS, G. 1968 Effect of a stabilizing gradient of solute on thermal convection. *J. Fluid Mech.* **34**, 315–336.